Precise Switching of Flagellar Gene Expression in *Escherichia Coli* by the FlgM–FliA Regulatory Network

Stephan Menz[1#], Reiner Matthiesen[1#], Christof Dehmel[1], Claudia Barembruch[2], Regine Hengge[2], Wilhelm Huisinga[3,*],

1 Department of Mathematics and Computer Science, Freie Universität Berlin, Berlin, Germany
2 Department of Biology, Chemistry and Pharmacy, Freie Universität Berlin, Berlin, Germany
3 Hamilton Institute, National University of Ireland, Maynooth, Co. Kildare, Ireland
∗ E-mail: Wilhelm.Huisinga@nuim.ie
 # These authors contributed equally to this work.

Abstract

A remarkable feature of flagellar synthesis in *Escherichia coli* is that gene expression is sequential and coupled to the assembly process. The interaction of two key proteins, the flagellar sigma factor FliA and its anti-sigma factor FlgM serves as a major checkpoint in the assembly process that temporally separates middle and late gene expression. While the sequential nature within each gene class has been studied using large-scale transcriptional data, much less is known about the timing controlled by the checkpoint mechanism. In this article, we analyze timing, sensitivity and robustness of the FlgM–FliA core regulatory mechanism based on quantitative molecule data and a detailed stochastic as well as reduced deterministic reaction kinetics model. We find that the pool of free anti-sigma factor FlgM, accumulated during middle gene expression, acts as a molecular timer that determines the delay between successful completion of the hook basal body subunit and the start of expression of flagellar filament proteins. Furthermore, we find that the number of free FliA molecules needs to be tightly controlled for a precise switch from middle to late gene expression. A sensitivity analysis based on the reduced reaction kinetics model reveals that the checkpoint mechanism is very sensitive to changes in levels of competing sigma factors, allowing the bacterium to rapidly adapt to a changing environment. In addition, we find that the reduced model also shows a high sensitivity to the effective synthesis rates of FliA and FlgM. However, this high sensitivity does not generally carry over to the original parameters of transcriptional and translational processes in the detailed model. As a consequence, care has to be taken whenever interpreting results from the robustness analysis of reaction kinetic models comprising lumped or effective parameters. (Currently 289 words)

Author Summary

The bacterial flagellum is a rotary motor that enables bacteria like E. coli to swim in a liquid environment. A remarkable feature of flagellar biosynthesis is that gene expression is coupled to the assembly process, which triggers a molecular checkpoint mechanism controlling gene expression. Flagellar gene expression is arranged in a specific temporal hierarchy, and divided into early, middle and late genes according to the assembly process. The interaction of two flagellar proteins, FlgM and FliA, serves as a major checkpoint, signalling the switch from middle to late gene expression. Here, we study the FlgM–FliA regulatory mechanism in detail, based on quantitative molecule data and reaction kinetics models. Our results provide novel insight into the molecular checkpoint and reveal how E. coli manages to ensure robustness of the signalling system and, at the same time, to maintain its ability to adapt to a changing environment.

Introduction

Escherichia coli (*E. coli*) is a non-differentiating bacterium that exhibits very different 'life-styles': The bacteria can occur as single planktonic and motile cells or they can exist as multicellular sessile aggregates, i.e., in biofilms [1–6]. The motile state is dependent on properly controlled biosynthesis of flagella that are complex rotating organelles anchored in the cell envelope. The flagella comprise three parts—the basal body, the hook, and the filament—that are sequentially assembled from the base to the distal end [7]. A remarkable aspect of flagellar assembly in *E. coli* is that gene expression is temporally ordered and coupled to the assembly process [8]. The same has been observed for other bacteria, like *Salmonella typhimurium* [9].

The flagellar gene regulation cascade of *E. coli* consists of more than sixty genes that are organized in three hierarchically and temporally regulated transcriptional classes [10–12]. Global regulators feed into a single class 1 promotor which leads to the initiation of flagellar synthesis. The class 1 (early) genes code for the subunits of the transcription factor FlhDC, the flagellar master regulator, that subsequently activates class 2 promotors [12, 13]. The protein products of the class 2 (middle) genes are structural components of the flagellar hook basal body, as well as the transcriptional regulators FliA and FlgM. FliA is an alternative sigma factor (σ^{F}) that enables transcription of the class 3 (late) genes which encode the proteins for the flagellar filament and the control of motility and chemotaxis [14, 15]. In the middle phase of flagellar assembly, FliA is actively inhibited by FlgM, its anti-sigma factor, that tightly binds to FliA.

With the hook basal body, a type III secretion system is formed that is necessary for the secretion of the flagellar filament subunits [7, 16]. The hook basal body enables also FlgM export from the cell with FliA also acting as a chaperone that delivers FlgM to the export machinery. [17]. The FliA-mediated export of FlgM results in the release of FliA from the FlgM:FliA complex, an increase in free FliA levels and eventually in activation of class 3 transcription [18]. In this way, class 3 gene expression of filament proteins is coupled to the assembly process of the hook basal body.

While the sequential nature of middle and late gene expression has been studied using real-time monitoring of transcriptional activation based on β-galactosidase [4] and green fluorescent protein [8,19] fusion measurements, the dynamics of the FlgM–FliA checkpoint mechanism and of the switch from middle to late gene expression are only poorly understood. The objective of this article is to analyze the timing and robustness of the FlgM–FliA core regulatory mechanism. Since regulation based on protein-protein interaction can not be studied by means of gene transcription data, we used quantitative measurements of FliA and FlgM protein numbers over time [4] to develop and validate a detailed stochastic model of the transcriptional, translational and protein-interaction processes that are relevant for the FlgM–FliA checkpoint mechanism. The stochastic reaction kinetics model accounts for statistical fluctuations due to small numbers of molecules, as well as the asynchrony in the cell culture before induction. The core regulatory mechanism is subsequently studied based on a reduced deterministic model that is derived and parameterized from the detailed stochastic model. Our results provide new insight into the timing of the checkpoint mechanism. Since flagella are a common and conserved motive among mobile bacteria [20], our results are expected to have implications beyond the present study.

Results

Development of the Detailed Stochastic Model

Model Description

We developed a detailed mathematical model of the gene regulatory cascade involved in flagellar synthesis based on the biological model shown in Fig. 1.

The input of the model is the induced synthesis of FlhDC complex—analogous to the experimental realizations in [4]. The FlhDC master regulator acts as a transcription factor that reversibly binds to the class 2 operons *flgAMN* and *fliAZY* that encode for FlgM and FliA, respectively. If activated, σ^{D}:RNAP complexes can reversibly bind to the operons and class 2 gene expression gets initiated (a σ^{D}:RNAP complex is formed by reversible binding of σ^{D} to the core enzyme RNAP). After initiation and elongation (according to the length of the gene) the corresponding $mRNA_{flgAMN}$ and $mRNA_{fliAZY}$ are released. Both mRNAs are subject to degradation. Initiation and elongation of the translation of $mRNA_{flgAMN}$ and $mRNA_{fliAZY}$ eventually results in the successful synthesis of FlgM and FliA molecules, respectively. The sigma factor and its anti-sigma factor reversibly bind to form the FlgM:FliA complex. The number of free FliA molecules is reduced by proteolysis, mediated mainly by Lon-protease. In addition, all molecular species are subject to dilution due to cell growth and cell division. The cell culture is assumed to be asynchronous, i.e., the cells can be in different stages of the cell cycle.

After completion of a hook basal body, FliA acts as a class III chaperon and delivers FlgM from the FlgM:FliA complex for export into the extra-cellular space. The specific export of FlgM from the complex results in a free FliA molecule in the cell interior. Free FliA can reversibly bind to the RNAP core enzyme to form the σ^{F}:RNAP complex, necessary for transcription of class 3 genes. A σ^{F}:RNAP complex reversibly binds to various class 3 operons including *flgMN* and *fliAZY* encoding for FlgM and FliA, respectively. After initiation and elongation (according to the length of the gene) of class 3 gene expression the corresponding class 3 $mRNA_{flgMN}$ and $mRNA_{fliAZY}$ are released. Both mRNAs are again subject to degradation.

The detailed list of reactions is given in the Supporting Information. We choose the stochastic formulation of biochemical reaction kinetics [21, 22], which was extended to correctly account for volume changes during an asynchronously simulated cell growth and cell division [23], to simulate the overall transcription–translation–protein interaction network. This allowed us to account for the discrete nature of reaction events in the presence of small numbers of molecules (e.g., free FliA or σ^{F}:RNAP), as well as a sufficiently detailed model of gene transcription and translation (including initiation and elongation). Alternatively, the deterministic formulation of biochemical reaction kinetics based on the law of mass action could have been chosen. However, for detailed models of gene transcription the stochastic formulation seemed to us the more natural one, being closer to the biological model and language. In addition, it not only makes predictions about the mean behavior, but also about the expected variability.

Parameterization and Validation of the Model

The detailed stochastic reaction kinetic model was parameterized based on *in vivo* data from *E. coli* or related bacteria (this applied to the majority of parameters, including all key parameters). When *in vivo* data were not available, data were taken from *in vitro* measurements. Only three parameters could not be obtained by *in vivo* or *in vitro* measurements, and were therefore estimated based on our experimental measurements for the wild type strain [4]: the synthesis rate of FlhDC, the export rates of FlgM, and the class 2 transcription initiation rate of *fliAZY*. The full list of experimental and estimated parameter values as well as the initial molecular numbers are listed in Table S1 and S2 in the Supporting Information.

Wild type: The experimental data of intra-cellular and extra-cellular FlgM as well as intra-cellular FliA is shown in Fig. 2A–C, marked with '*', together with the model predictions of the median (solid line), the area between the 40^{th} and 60^{th} percentile (dashed lines) and the area between the 1^{st} and 3^{rd} quartile ($25^{\mathrm{th}}/75^{\mathrm{th}}$ percentile, dotted lines). The model predictions (mean as well as variance) are in good agreement with our experimental data [4] and other experimental findings [18].

Upon induction, the FlhDC level begin to rise (data not shown) and FlhDC activates the transcription of the class 2 operons. This results in an increase in molecular numbers of FlgM and FliA. After

around 22 min, the first hook basal bodies are completed and FlgM begins to be exported to the extracellular space, resulting in a continuous increase in extra-cellular FlgM, as shown in Fig. 2B. While FliA continues to increase (see Fig. 2C), the model predicts a noticeable transient decrease in intracellular FlgM until eventually newly synthesized FlgM molecules resulting from class 3 gene expression increase the molecular numbers again (see Fig. 2A). The model predictions excellently reproduce the mean as well as the variability of FlgM over time (see, e.g., the growing experimental variability in external FlgM over time). Regarding FliA, the model slightly underestimates the initial increase in FliA measured experimentally, while the initial base line levels as well as the final numbers are again in perfect agreement with the experimental data (see Fig. 2C; please, see Discussion for a potential explanation).

***flgM*$^-$ mutant:** Since the *flgM*$^-$ mutant by design lacks FlgM, experimental measurements compared to model prediction are only shown for FliA in Fig. 2D. The *in silico* predictions of FliA levels are in excellent agreement with experimental data. The FliA levels are roughly half the size in comparison to the wild type levels, which is a consequence of FliA not being protected against proteolysis by forming the FlgM:FliA complex with FlgM.

Class 3 Gene Expression is Induced only when Pool of Free FlgM is Drastically Reduced

We next studied in detail the checkpoint mechanism based on the stochastic model. In contrast to the experimental measurements, the model allowed us to distinguish between free and bound FliA, as well as to monitor the predicted σ^F:RNAP number of molecules in order to study the onset of class 3 expression. The predictions for the wild type are shown in Fig. 3A for free FlgM, free FliA and FlgM:FliA (left axis) and σ^F:RNAP (right axis) for the relevant time span from 10-40 min.

Experimentally, it has been shown that FlgM is exported from the FlgM:FliA complex with FliA acting as a type III secretion chaperone [17]. *In silico*, however, the most pronounced change in terms of numbers of molecules is the rapid decrease in free FlgM upon completion of the export apparatus around 22 min, but not as one might intuitively expect in the level of FlgM:FliA complexes.

A closer look at key reactions resolves this surprising behavior: The export of FlgM from the FlgM:FliA complex significantly increases with the completion of the export apparatus. Since FliA is released from the complex when FlgM is exported, the availability of free FliA significantly increases. However, due to the high affinity of FliA for FlgM, it immediately forms a new complex with a free FlgM. Hence, FliA-mediated export of FlgM effectively decreases the level of free FlgM, with the FlgM:FliA complexes remaining at high levels, but having a very short life span and being 'produced just in time' for the export.

The tight balance of FlgM–FliA association, FlgM export and FliA release results in extremely low levels of free FliA during the first minutes of the export (see Fig. 3). With continued export and decreasing levels of free FlgM, this balance is perturbed towards increasing free FliA levels. Although this increase is only marginal between 22-27 min, it is sufficient to form the first σ^F:RNAP complexes that initiate class 3 expression. This transient phenomenon was already present in the total intra-cellular number of FlgM molecules, as shown in Fig. 2A. As we remarked, the number of FlgM transiently decreases upon start of export. Based on the above analysis, we may now associate this transient decay with the decrease in the pool of *free* FlgM. Only when this pool is strongly reduced, class 3 expression can be initiated.

In Fig. 3B, the timing of wild type and *flgM*$^-$ mutant is compared. Due to lack of FlgM in the mutant, rising FliA levels during class 2 gene expression immediately initiate class 3 expression (note that the σ^F:RNAP scale is relative to basal level for easier comparison).

In the following, we studied in more detail the robustness of the FlgM–FliA checkpoint mechanism, including the relation between the reduction of the free FlgM pool and formation of σ^F:RNAP complexes—considered as the indicator for class 3 initiation.

Model Reduction to the Core Regulatory Mechanism

For the in-depth study of the FlgM–FliA regulatory network and its robustness, we reduced the detailed stochastic model to its core regulatory mechanism on the protein–protein interaction level. The direct interactions between FlgM and FliA involves only large numbers of molecules, and since transcriptional and translational processes were lumped into an effective synthesis rate, we choose the deterministic formulation of biochemical reaction kinetics. Cell growth and division were represented by an effective dilution rate constant. See 'Materials and Methods' section for details on the reduction process.

Reduced Deterministic Model

In the reduced model, FlgM and FliA are synthesized with effective rate constants k_{FlgM} and k_{FliA}, respectively. For FlgM, class 2 and class 3 expression was taken into account, while for FliA only class 2 expression was considered, since class 3 expression is comparably small (see Materials and Methods). FlgM and FliA are subject to dilution during cell growth and division, represented by the effective rate constant k_{dil}. In addition, FliA is proteolysed with rate constant k_4. The sigma factor FliA and its anti-sigma factor FlgM form a complex with association and dissociation rate constants k_9 and k_{10}, respectively. After completion of the hook basal body, FlgM is exported from the FlgM:FliA complex with rate constant $k_{11}(t)$, with FliA remaining in the intra-cellular space. Finally, FliA (σ^{F}) forms a complex with RNAP with association and dissociation rate constants k_{14} and k_{15}, respectively. The rates of change of the molecular species FlgM, FliA, FlgM:FliA and extra-cellular $\mathrm{FlgM}_{\mathrm{extern}}$ are given by the following system of ordinary differential equations (ODEs):

$$\begin{aligned}
\frac{d}{dt}\mathrm{FlgM} &= k_{\mathrm{FlgM}}(t) - (k_9 \cdot \mathrm{FliA} + k_{dil}) \cdot \mathrm{FlgM} \\
&\quad + k_{10} \cdot \mathrm{FlgM{:}FliA} \\
\frac{d}{dt}\mathrm{FliA} &= k_{\mathrm{FliA}}(t) + (k_{10} + k_{11}(t)) \cdot \mathrm{FlgM{:}FliA} + k_{15} \cdot \sigma^{\mathrm{F}}{:}\mathrm{RNAP} \\
&\quad - (k_4 + k_9 \cdot \mathrm{FlgM} + k_{14} \cdot \mathrm{FliA} \cdot \mathrm{RNAP} + k_{dil}) \cdot \mathrm{FliA} \\
\frac{d}{dt}\mathrm{FlgM{:}FliA} &= k_9 \cdot \mathrm{FlgM} \cdot \mathrm{FliA} - (k_{10} + k_{11}(t) + k_{dil}) \cdot \mathrm{FlgM{:}FliA} \\
\frac{d}{dt}\mathrm{FlgM}_{\mathrm{extern}} &= k_{11}(t) \cdot \mathrm{FlgM{:}FliA} - k_{dil} \cdot \mathrm{FlgM}_{\mathrm{extern}}.
\end{aligned}$$

In the above system of ODEs, free RNAP and σ^{F}:RNAP enter the equations. In principle, the level of free RNAP and the output level of σ^{F}:RNAP could be approximated from the total levels of RNAP and σ^{D} and the corresponding association/dissociation constants. However, we choose to explicitly integrate σ^{D} in the reduced model such that we could study the competition of sigma-factors for free RNAP. For this purpose, the above system of ODEs was amended by the ODEs for the rates of change of σ^{F}:RNAP, σ^{D}:RNAP, σ^{D} and free RNAP:

$$\begin{aligned}
\frac{d}{dt}\sigma^{\mathrm{F}}{:}\mathrm{RNAP} &= k_{14} \cdot \mathrm{FliA} \cdot \mathrm{RNAP} - (k_{15} + k_{dil}) \cdot \sigma^{\mathrm{F}}{:}\mathrm{RNAP} \\
\frac{d}{dt}\sigma^{\mathrm{D}}{:}\mathrm{RNAP} &= k_{12} \cdot \sigma^{\mathrm{D}} \cdot \mathrm{RNAP} - k_{13} \cdot \sigma^{\mathrm{D}}{:}\mathrm{RNAP} \\
\frac{d}{dt}\sigma^{\mathrm{D}} &= -\frac{d}{dt}\sigma^{\mathrm{D}}{:}\mathrm{RNAP} \\
\frac{d}{dt}\mathrm{RNAP} &= -\frac{d}{dt}\sigma^{\mathrm{D}}{:}\mathrm{RNAP} - \frac{d}{dt}\sigma^{\mathrm{F}}{:}\mathrm{RNAP}.
\end{aligned}$$

The above system of ODEs models the formation of the σ^{D}:RNAP complex with association and dissociation rate constants k_{12} and k_{13}, respectively. In addition, σ^{F}:RNAP is subject to dilution with rate constant k_{dil}. The average number of σ^{D} and RNAP molecules was assumed to be constant in the detailed stochastic model and their dilution has been compensated by equivalent synthesis reactions (see Supporting Information). Therefore, we could simply omitt the dilution and synthesis of σ^{D} and RNAP in the above ODEs.

Reactions in the reduced model that are also present in the detailed model were parameterized with the same rate constants and parameter values. These were all rate constants except for: the rate constants of effective FliA and FlgM synthesis k_{FlgM} and k_{FliA}, respectively and the dilution rate constant k_{dil}. These three rate constants were derived from the detailed stochastic model by a mechanistic model reduction process; for details see Materials and Methods. No additional parameter estimation was performed for the reduced model. We remark that a *de novo* parameterization of the reduced deterministic model would require to estimated the same number of parameters estimated for the detailed stochastic model. A complete list of parameter values for the reduced model is given in Table 1.

Validation of the Reduced Deterministic Model

We validated the reduced deterministic model against the experimental data of the wild type and *flgM*$^-$ mutant as well as against the predicted mean of the detailed stochastic model. The predicted levels of FliA and FlgM are in very good agreement with the predictions based on the detailed stochastic model (see Fig. 4). We observed a slightly more rapid increase in molecular numbers compared to the detailed stochastic model, since a temporal delay resulting from the transcriptional and translational reactions can not be reflected in the effective synthesis rate constants of the reduced deterministic model (unless explicitly modeled by a delay differential equation).

Robustness and Timing of the Core Regulatory Mechanism

We used the reduced deterministic model to analyze the robustness of the FlgM–FliA checkpoint regulatory mechanism to tightly control σ^{F}:RNAP level, as this is the critical marker for class 3 gene expression initiation. Wild type levels were compared to levels of *in silico* mutants with 'perturbed' parameter values in order to access the robustness with respect to the alterations.

Checkpoint is Robust to Perturbations in FlgM–FliA Association and Dissociation

Levels of σ^{F}:RNAP for wild type and *in silico* mutants with increased FlgM:FliA dissociation rate constant (1-, 100-, 500- and 1000-fold increase compared to the wild type) are shown in Fig. 5A and inset. Changes of up to 3 orders of magnitude have only marginal influence on σ^{F}:RNAP levels, thus rendering the regulatory network robust with respect to the binding affinity of FlgM and FliA.

FliA Proteolysis and Sigma Factor Competition for RNAP Modulate Intensity of Class 3 Gene Expression Initiation

The intensity of initiation of class 3 gene expression is directly related to the available level of σ^{F}:RNAP complexes. Fig. 5B shows the decrease in σ^{F}:RNAP levels resulting from an increase in the FliA (σ^{F}) proteolysis rate constant. Increased proteolysis results in decreased levels of σ^{F} and consequently in decreased levels of σ^{F}:RNAP. In Fig. 5C and D, the wild type levels were compared to that with decreased (C) and increased (D) levels of sigma factor σ^{D}. Both *in silico* experiments directly alter the competition of sigma factors for RNAP, where the regulatory mechanism is extremely sensitive to. In all three cases, the considered *in silico* settings modulate the steepness of increase in σ^{F}:RNAP levels and hence the total level available for class 3 transcription, most notably when altering the competition of sigma factors for RNAP.

Pool of Free FlgM Precisely Controls Free FliA Level and Acts as a *Molecular Timer*

We have seen in Fig. 2 that the class 3 initiation is coupled to the reduction of the pool of accumulated free FlgM. Since alteration in the FlgM export rate and the time when the export starts directly affect this timing, we would expect to see a change in the initiation of class 3 gene expression due to alteration in these two parameters. As illustrated in Fig. 6, this is the case. The checkpoint mechanism is indeed sensitive to the FlgM export rate and the time when the export starts. Perturbations in these two parameters affect both the rate at which σ^{F}:RNAP complexes increase, and the point in time when the increase of σ^{F}:RNAP starts.

In addition to the level of σ^{F}:RNAP, the level of free FlgM are shown in Fig. 6. Changes in the above processes have a direct influence on the accumulation of free FlgM and the decay of the FlgM pool. As is nicely illustrated in Fig. 6, σ^{F}:RNAP complexes do not begin to increase until all excessive *free* FlgM is exported from the cell. In this sense, the pool of free FlgM acts as a *molecular timer* that precisely controls the start of σ^{F}:RNAP formation and therefore class 3 expression.

High Sensitivity of Effective Synthesis Rates in the Reduced Model, but Low Sensitivity with respect to the Subsumed Parameters of the Detailed Model

A change in the synthesis rate of FlgM or FliA alters the ratio between FlgM and FliA levels in the system, thus re-weighting the pool of free FlgM and its function as a molecular timer. Therefore, we expected that class 3 gene expression would start later or earlier when compared to the wild type. This can be seen in Fig. 7, were we analyzed the sensitivity of the checkpoint mechanism to alterations in the effective synthesis rates k_{FlgM} and k_{FliA}. An increased synthesis rate of FlgM resulted in an increase pool of free FlgM, thus increasing the delay from start of export to class 3 initiation (1.4-fold change, green). The opposite effect occurred for a decreased synthesis rate of FlgM (0.7-fold change, yellow). An increased synthesis rate of FliA diminished the pool of *free* FlgM by increasing the level of the FlgM:FliA complexes, thus decreasing the delay from start of export to class 3 initiation (1.4-fold change, green). Again, the opposite effect occurred for a decreased synthesis rate of FliA (0.7-fold change, yellow). The results illustrated in Fig. 7A and B suggest that the checkpoint mechanism is as sensitive to alterations in the synthesis rates as it is to alterations to FlgM export rate or the time when the export starts.

However, since the synthesis rates of FliA and FlgM in the deterministic model are effective rates subsuming complex reaction events of gene transcription and translation, we analyzed the effect of the model reduction process on the observed sensitivity, i.e., we studied whether the same sensitivity on σ^{F}:RNAP levels can be observed when altering the original parameters of the processes that were subsumed in the effective synthesis rates (cf. Eqs. (1) and (2) in Materials and Methods). To this end, we considered the reaction parameters of the binding/dissociation rates of FlhDC to class 2 promoters and the initiation rates of transcription and translation.

As can be inferred from Fig. 7C and D, a high sensitivity of σ^{F}:RNAP levels to alterations in the effective synthesis rates k_{FlgM} and k_{FliA} does not necessarily imply a high sensitivity with respect to alterations in the subsumed gene expression parameters in the detailed stochastic model. The synthesis rate of FlgM subsumed both class 2 and class 3 gene expression, including the effects of each of the transcriptional and translational reaction events. Therefore, an alteration in, e.g., class 2 transcription has only a minor influence on the total synthesis rate (see Fig. 7C), since it constitutes only a fraction of the total transcription (comprising class 2 and 3). In contrast, the FliA synthesis rate only subsumes class 2 expression (since class 3 expression was negligible). Hence, a slightly stronger dependence on alteration in class 2 transcription parameters can be observed (see Fig. 7D). In total, a change in parameters accounting for the transcriptional processes has a smaller impact on σ^{F}:RNAP levels than alterations in parameters accounting for translational processes, e.g., the translation initiation rate constants. Changes in translational parameters correspond 1:1 to changes in the effective synthesis rate of FliA, while a weaker correlation was observed for the synthesis rate of FlgM due to the mentioned existence of class 2

and class 3 gene expression. This exactly would we expected in view of Eqs. (1) and (2) in Materials and Methods.

Hence, the sensitivity of the initiation of class 3 gene expression with respect to the effective synthesis rates of FlgM and FliA is largely an artefact of the reduction process that subsumed detailed transcriptional and translational reaction events into effective synthesis rates. This phenomenon is not restricted to the present analysis, and as a consequence, care has to be taken when interpreting results of robustness analysis of general reaction kinetic models comprising lumped or effective parameters.

Discussion

In this study, we have analyzed the FlgM–FliA regulatory network that controls the transition from class 2 to class 3 gene expression in the flagellar synthesis of *E. coli*. All in all, the model predictions are consistent with existing experimental data and knowledge, which justifies confidence in the overall modeling process. The number of σ^{F}:RNAP holoenzyme is the critical parameter controlling the initiation of class 3 gene expression—and hence, a tight control of σ^{F}:RNAP is required for a controlled and efficient synthesis of new flagella.

Before successful completion of the first hook basal bodies and subsequent start of FliA-mediated export of FlgM, the sigma factor FliA (σ^{F}) is sequestered in the FlgM:FliA complex in its inactive form, since only free FliA can bind to the core enzyme RNAP. Control of initiation of class 3 expression is implemented by maintaining a certain stoichiometric ratio between FlgM and FliA. Upon start of export, the pool of free FlgM is gradually degraded until a change in the stoichiometric ratio between FlgM and FliA results in a sufficient number of free FliA molecules to enable class 3 initiation (Fig. 6). In the absence of FlgM, this delay is not present and class 3 expression is closely following the increase of FliA levels (Fig. 3B).

In our reduced deterministic model, an increase in the number of successfully completed hook basal bodies would correspond to an increase of the FlgM export rate. As shown in Fig. 6A, this directly decreases the delay between start of export and class 3 initiation. In [8] experimental evidence is given that when preexisting flagella are present, newly synthesized FlgM is already exported before new basal bodies have been completed. As a consequence, less free FlgM can accumulate. The dynamic control of the pool of free FlgM presented herein could serve as a mechanistic explanation of this experimental observation. This also highlights that the relative ratio of FlgM to FliA is important for the functionality of the checkpoint mechanism.

Robustness is one of the fundamental characteristics of biological systems, as is the ability to rapidly adapt to a changing environment [24,25]. *In silico*, the underlying questions of robustness and adaptation: "How sensitive is the model to perturbations in the input?" is typically addressed based on a sensitivity analysis of the predicted output in terms of the model input.

The analysis of the FlgM–FliA regulatory mechanism reveals that the system is robust to alterations of most of the parameters (Fig. 5A and B, Fig. 7C and D), while it is sensitive to alterations of those inputs that are exploited by *E. coli* to adapt and tune the mechanism in face of a changing environment. These correspond either to parameters that allow *E. coli* to tune initiation of class 3 expression, e.g., in terms of strength or start of export (Fig. 6), or that serve as the point of entry of other master regulators. The increase of σ^{F}:RNAP, considered as a marker for class 3 expression, is most notably affected by alterations in the sigma factor competition (Fig. 5C and D). This tuning point allows for a direct, efficient and instantaneous alteration of flagellar synthesis, which is, e.g., important in the transition from the motile-planktonic to the stationary phase 'lifestyle', that is induced by the accumulation of the σ^{S} subunit of RNAP [6, 26].

Care has to be taken when addressing the question of robustness and sensitivity in terms of effective parameters. While the checkpoint mechanism shows sensitivity to alterations in the effective synthesis rates of its key molecular species FlgM and FliA (Fig. 7A and B), this sensitivity does in general not

persist when analyzing the sensitivity of σ^F:RNAP levels in terms of the original parameters that are subsumed in the effective rate constants (see Fig. 7C and D, and Eqs. (1) and (2) in Materials and Methods). Only the initiation rate constant of FliA class 2 translation showed the same sensitivity (Fig. 7D, k_{41}); which suggests that this parameter is also controlled *in vivo*.

The *in silico* levels of intra- and extra-cellular FlgM in the wild type as well as FliA level in the *flgM*$^-$ mutant are in excellent agreement with the *in vivo* data (Figs. 2 and 4). In the wild type, however, the model slightly underestimates the experimentally observed steep increase of the FliA level (Fig. 2C). In addition to the FlgM–FliA checkpoint, there exists a number of interlocking positive and negative feedback loops with the potential to further modulate class 2 and class 3 expression [9, 27, 28], including the FliT–FliD regulatory system [27, 28]. FliT is the secretion chaperone for the filament capping protein FliD. Upon completion of the hook basal body, FliD is secreted to the tip of the hook where it facilitates polymerizaton of the flagellar filament [28]. The depletion of FliD from the cytoplasm eventually results in increased levels of *free* FliT. Free FliT subsequently binds to FlhC and thereby inhibits transcription of the middle genes whose products are no longer required for the assembly process [27]. Due to lack of *quantitative* experimental data, this additional regulatory mechanism is absent in the proposed model.

We expect that inclusion of the FliT–FliD feedback would result in larger initiation rates for FliA transcription in the parameter estimation process (FliA initiation rate was one of the three parameters estimated from the wild type data). This would result in a stronger initial increase of FliA levels during class 2 expression. Upon completion of the hook basal body, FliD export would than result in increasing levels of FliT that subsequently slow down class 2 gene expression. The actual implementation and potential impact of other molecular species, however, has to be left to future experimental and theoretical studies. Experimentally, this might be challenging to verify, since the number of FliD molecules is expected to be very low.

Importantly, the FliT–FliD regulatory system is expected to exhibit the same characteristics as the FlgM–FliA checkpoint mechanism. The herein presented analysis and results may therefore serve as a starting point for future experimental design and theoretical studies.

Similar or analogous checkpoint mechanism are present in many other motile bacteria [20]. In *Salmonella typhimurium*, both FlgK and FlgL bind to FlgN and inhibit its regulatory activity, suggesting that FlgN is also involved in a checkpoint coupled to completion of the hook basal body, similarly to the FlgM–FliA regulatory system [29]. The bacterial injectisome (or needle complex) is structurally similar to the flagellum and consists of a basal body-like structure, an associated secretion system, and a hollow needle-like filament that protrudes from the cell surface and serves as the conduit through which proteins are secreted [28]. Much like the flagellum, assembly of the injectisome is thought to proceed in a sequential manner starting with formation of a basal structure and ending with export of the needle protein to the distal tip.

In *E. coli*, both motility and biofilm formation are under control of regulatory feed forward cascades with mutual interaction and cross-regulation at different levels [6, 26]. In this context the proposed model may be seen as a first step towards a more comprehensive model of life style adaptation in *E. coli*, describing the programmed succession of a foraging strategy with transiently increased motility [3] followed by induction of the general stress response mainly directed towards maintenance and stress survival [26,30,31] as well as adhesion and biofilm formation during entry into stationary phase [5]. While experimental data on gene transcription or promoter activity may provide further insight in the temporal hierarchy of gene expression, more quantitative data in terms of molecular numbers combined with mathematical modeling and analysis are needed to analyze the regulatory processes on the proteinprotein interaction level.

Materials and Methods

Experimental Setup

The generation of experimental data such as *in vivo* FliA and FlgM levels, rates of FliA degradation and class 2 and 3 gene expression in various genetic backgrounds has been described in detail in [4]. A full description of the detailed stochastic model is given in the Supporting Information. The stochastic reaction kinetics has been implement in C++. All further computations were performed in *Mathematica*®.

Simulation of Cell Growth and Asynchronous Cell Cultures

All *in silico* studies comprise an ensemble of 1000 realizations, where every single simulation can be understood as representing an individual cell in an asynchronous cell culture. For this purpose, we included cell growth and cell division in the model. The cell growth was realized by linearly doubling the cell volume in a period of 24 min (in accordance with the growth conditions of the experimental setup in [4]). When the volume reached an assumed maximal value of $2.66 \cdot 10^{-15} l$, we simulated cell division, i.e., bisected the volume and all molecule numbers.

Asynchronous cell cultures were simulated by initializing each realization at a randomly chosen state of cell growth. According to this, the initial volume and molecule numbers of RNAP, σ^{D} and FlhDC were set with respect to their minimal values and rates of synthesis in cell growth (see Table S1 and S2 in the Supporting Information). We performed *in silico* experiments with up to 20 percent variability in cell growth and volume (data not shown), which, however, showed no significant changes in the predicted molecule levels.

Parameterization

In our experiments [4], the flagellar cascade was induced by activating *flhDC* expression from an inducible promoter (which produces FlhDC levels comparable to those in a wild type strain); subsequently molecular levels of FliA and intra- and extra-celular FlgM were measured at several time points (immediately upon induction, and 5, 20, 35, 50 and 80 min after induction). To resemble this *in vivo* experiment, we induced the flagellar signalling *in silico* by an increase in FlhDC, i.e., class 1 expression. In accordance to [4], we simulated two *in silico* situations:

- *Wild type.* Used for parameterization of the input signal, i.e., the FlhDC level, the initiation rates of the transcription reactions, and the export rates of FlgM. All parameters were set as specified in the Supporting Information; results are shown in Fig. 2A–C.
- *flgM- mutant.* Used for validation of the model. The reaction rates of the transcription initiations of FlgM were set to zero, thereby turning off class 2 and class 3 expression of FlgM; all other settings were as in the wild type. Results are shown in Fig. 2D.

All *in silico* studies involve an ensemble of 1000 realizations, visualized by its median (solid line), the area between the 40^{th} and 60^{th} percentile (dashed lines) and the area between the 1^{st} and 3^{rd} quartile ($25/75^{\mathrm{th}}$ percentile, dotted lines). Predicted molecular numbers are directly compared to the experimental data from [4], which are marked by '*' in Fig. 2.

Model reduction

In the detailed stochastic model, cell growth and division effectively results in a degradation of the molecular species. In the deterministic model, we represented this process by the expected dilution of each species. The rate constant k_{dil} is approximated by

$$k_{dil} = \frac{\ln(2)}{24 \cdot 60\,[s]} \approx 4.8 \times 10^{-4}\,\left[s^{-1}\right],$$

where $24 \cdot 60\,[s]$ is the mean length of the cell cycle in the stochastic model.

The effective synthesis rates of FliA and FlgM can be approximated from their average mRNA transcripts via

$$k_{\mathrm{FliA}} = k_{41} \cdot \mathrm{mRNA}^{*}_{\mathit{fliAZY_2}}, \tag{1}$$

$$k_{\mathrm{FlgM}}(t) = k_{40} \cdot \mathrm{mRNA}^{*}_{\mathit{flgAMN}} + k_{42} \cdot \mathrm{mRNA}_{\mathit{flgMN}}(t)\,, \tag{2}$$

where k_{40}, k_{41} and k_{42} are the specific translation initiation constants of the corresponding mRNA transcripts. The average mRNA transcripts are determined from the corresponding class 2 and 3 transcription rates (see Table S2 in Supporting Information)

$$k_{tr_{\mathit{fliAZY_2}}} = \frac{k^{*}_{18} k^{*}_{22} k_{29} k_{34}}{k^{*}_{18} k^{*}_{22} k_{29} n_{34} + k_{19} k_{34} \left(k_{23} + k_{29}\right) + k^{*}_{18} k_{34} \left(k^{*}_{22} + k_{23} + k_{29}\right)},$$

$$k_{tr_{\mathit{flgAMN}}} = \frac{k^{*}_{16} k^{*}_{20} k_{28} k_{32}}{k^{*}_{16} k^{*}_{20} k_{28} n_{32} + k_{17} k_{32} \left(k_{21} + k_{28}\right) + k^{*}_{16} k_{32} \left(k^{*}_{20} + k_{21} + k_{28}\right)},$$

$$k_{tr_{\mathit{flgMN}}} = \frac{k^{*}_{24} k_{30} k_{36}}{k^{*}_{24} k_{30} n_{36} + k_{36} \left(k^{*}_{24} + k_{25} + k_{30}\right)},$$

where $k_{16}^* = k_{16} \cdot \text{FlhDC}^*$, $k_{18}^* = k_{18} \cdot \text{FlhDC}^*$, $k_{20}^* = k_{20} \cdot \sigma^{\text{D}}\text{:RNAP}^*$, $k_{22}^* = k_{22} \cdot \sigma^{\text{D}}\text{:RNAP}^*$, and $k_{24}^* = k_{24} \cdot \sigma^{\text{F}}\text{:RNAP}^*$ denote the average binding rates of FlhDC, σ^{D}:RNAP and σ^{F}:RNAP, respectively, in the stochastic model, when these have reached their steady state levels during class 2 and class 3 expression. Considering degradation and dilution, we approximated the corresponding average steady state levels of the mRNA transcripts as

$$\begin{aligned}
\text{mRNA}^*_{\mathit{fliAZY}_2} &= k_{tr_{\mathit{fliAZY}_2}} \Big/ (k_7 + k_{dil}) \approx 3.6, \\
\text{mRNA}^*_{\mathit{flgAMN}} &= k_{tr_{\mathit{flgAMN}}} \Big/ (k_5 + k_{dil}) \approx 10.2, \\
\text{mRNA}_{\mathit{flgMN}}(t) &= k_{tr_{\mathit{flgMN}}} \Big/ (k_6 + k_{dil}) \cdot \frac{\sigma^{\text{F}}\text{:RNAP}}{\sigma^{\text{F}}\text{:RNAP}^*} \approx 14.0 \cdot \frac{\sigma^{\text{F}}\text{:RNAP}}{\sigma^{\text{F}}\text{:RNAP}^*},
\end{aligned}$$

where the class 3 transcript $\text{mRNA}_{\mathit{flgMN}}$ depends on the ratio of the actual level of σ^{F}:RNAP to its steady state level σ^{F}:RNAP*, determined to be σ^{F}:RNAP$^* \approx 38.1$. Class 3 expression of FliA was not included in the reduced deterministic model, since the average steady state level of the transcript was considered negligible ($\text{mRNA}^*_{\mathit{fliAZY}_3} \approx 0.3$). A summary of all parameter values used in the reduced model is given in Table 1.

Acknowledgments

SM would like to thank the Dahlem Research School (DRS) for their support. Work in the laboratory of RH has been supported by the DFG Priority Program "Proteolysis in Prokaryotes" (SPP 1132; He1556/10-3).

References

1. Adler J, Templeton B (1967) The Effect of Environmental Conditions on the Motility of *Escherichia coli*. Journal of General Microbiology 46: 175–184.
2. Amsler CD, Cho M, Matsumura P (1993) Multiple Factors Underlying the Maximum Motility of *Escherichia coli* as Cultures Enter Post-Exponential Growth. Journal of Bacteriology 175: 6238–6244.
3. Zhao K, Liu M, Burgess RR (2007) Adaptation in bacterial flagellar and motility systems: from regulon members to 'foraging'-like behavior in E. coli. Nucleic Acids Research 35: 4441–4452.
4. Barembruch C, Hengge R (2007) Cellular levels and activity of the flagellar sigma factor FliA of *Escherichia coli* are controlled by FlgM-modulated proteolysis. Molecular Microbiology 65: 76–89.
5. Weber H, Pesavento C, Possling A, Hengge R (2006) Cyclic-di-GMP-mediated signalling within the σ^s network of *Escherichia coli*. Molecular Microbiology 62: 1014–1034.
6. Hengge R (2009) Principles of c-di-GMP signalling in bacteria. Nature Rev Microbiol 7: 263–273.
7. Macnab RM (1999) The Bacterial Flagellum: Reversible Rotary Propellor and Type III Export Apparatus. Journal of Bacteriology 181: 7149–7153.
8. Kalir S, McClure J, Pabbaraju K, Southward C, Ronen M, et al. (2001) Ordering Genes in a Flagella Pathway by Analysis of Expression Kinetics from Living Bacteria. Science 292: 2080–2083.
9. Saini S, Aldridge PD, Rao CV (2009) Role of Feedback Loops in Regulating Flagellar Gene Expression Dynamics in *S. Typhimurium*. FOSBE : 48–51.
10. Macnab RM (1996) Flagella and motility. In: Neidhardt FC, Curtiss III R, Ingraham JL, Lin ECC, Low KB, et al., editors, *Escherichia coli* and *Salmonella*: Cellular and Molecular Biology, ASM Press, Washington D.C., volume 2. 2 edition, pp. 123–145.
11. Chilcott GS, Hughes KT (2000) Coupling of Flagellar Gene Expression to Flagellar Assembly in *Salmonella enterica* Serovar Typhimurium and *Escherichia coli*. Microbiology and Molecular Biology Reviews 64: 694–708.
12. Chevance FFV, Hughes KT (2008) Coordinating assembly of a bacterial macromolecular machine. Nature Rev Microbiol 6: 455–465.
13. Liu X, Matsumura P (1994) The FlhD/FlhC Complex, a Transcriptional Activator of the *Escherichia coli* Flagellar Class II operons. Journal of Bacteriology 176: 7345–7351.
14. Kundu TK, Kusano S, Ishihama A (1997) Promoter Selectivity of *Escherichia coli* RNA Polymerase σ^f Holoenzyme Involved in Transcription of Flagellar and Chemotaxis Genes. Journal of Bacteriology 179: 4264–4269.
15. Liu X, Matsumura P (1995) An alternative sigma factor controls transcription of flagellar class-III operons in *Escherichia coli*: gene sequence, overproduction, purification and characterization. Gene 164: 81–84.
16. Hughes KT, Gillen KL, Semon MJ, Karlinsey JE (1993) Sensing structural intermediates in bacterial flagellar assembly by export of a negative regulator. Science 262: 1277–1280.

17. Aldridge PD, Karlinsey JE, Aldridge C, Birchall C, Thompson D, et al. (2006) The flagellar-specific transcription factor, σ^{28}, is the Type III secretion chaperone for the flagellar-specific anti-σ^{28} factor FlgM. Genes & Development 20: 2315–2326.
18. Karlinsey JE, Tanaka S, Bettenworth V, Yamaguchi S, Boos W, et al. (2000) Completion of the hook–basal body complex of the *Salmonella typhimurium* flagellum is coupled to FlgM secretion and *fliC* transcription. Molecular Microbiology 37: 1220–1231.
19. Kalir S, Alon U (2004) Using a Quantitative Blueprint to Reprogram the Dynamics of the Flagella Gene Network. Cell 117: 713–720.
20. Liu R, Ochman H (2007) Origins of Flagellar Gene Operons and Secondary Flagellar Systems. Journal of Bacteriology 189: 7098–7104.
21. Gillespie DT (1976) A general method for numerically simulating the stochastic time evolution of coupled chemical reactions. J Comput Phys 22: 403–434.
22. Turner TE, Schnell S, Burrage K (2004) Stochastic approaches for modelling in vivo reactions. Computational Biology and Chemistry 28: 165–178.
23. Alfonsi A, Cancès E, Turinici G, Ventura BD, Huisinga W (2005) Exact simulation of hybrid stochastic and deterministic models for biochemical systems. ESAIM: Proc 14: 1–23.
24. Stelling J, Sauer U, Szallasi Z, III FJD, Doyle J (2004) Robustness of cellular functions. Cell 118: 675–685.
25. Kitano H (2007) Towards a theory of biological robustness. Molecular Systems Biology 3: 1–7.
26. Pesavento C, Becker G, Sommerfeldt N, Possling A, Tschowri N, et al. (2008) Inverse regulatory coordination of motility and curli-mediated adhesion in *Escherichia coli*. Genes & Development 22: 2434–2446.
27. Yamamoto S, Kutsukake K (2006) FliT Acts as an Anti-$FlhD_2C_2$ Factor in the Transcriptional Control of the Flagellar Regulon in *Salmonella enterica* Serovar Typhiumurium. Journal of Bacteriology 188: 6703–6708.
28. Brutinel ED, Yahr TL (2008) Control of gene expression by type III secretory activity. Current Opinion in Microbiology 11: 128–133.
29. Brown JD, Saini S, Aldridge C, Herbert J, Rao CV, et al. (2008) The rate of protein secretion dictates the temporal dynamics of flagellar gene expression. Molecular Microbiology 70: 924–937.
30. Hengge-Aronis R (2000) The general stress response in *Escherichia coli*. In: Storz G, Hengge-Aronis R, editors, Bacterial Stress Response, ASM Press, Washington, DC. pp. 161–178.
31. Nyström T (2004) Stationary-Phase Physiology. Annual Review of Microbiology 58: 161–181.

Figure Legends

Tables

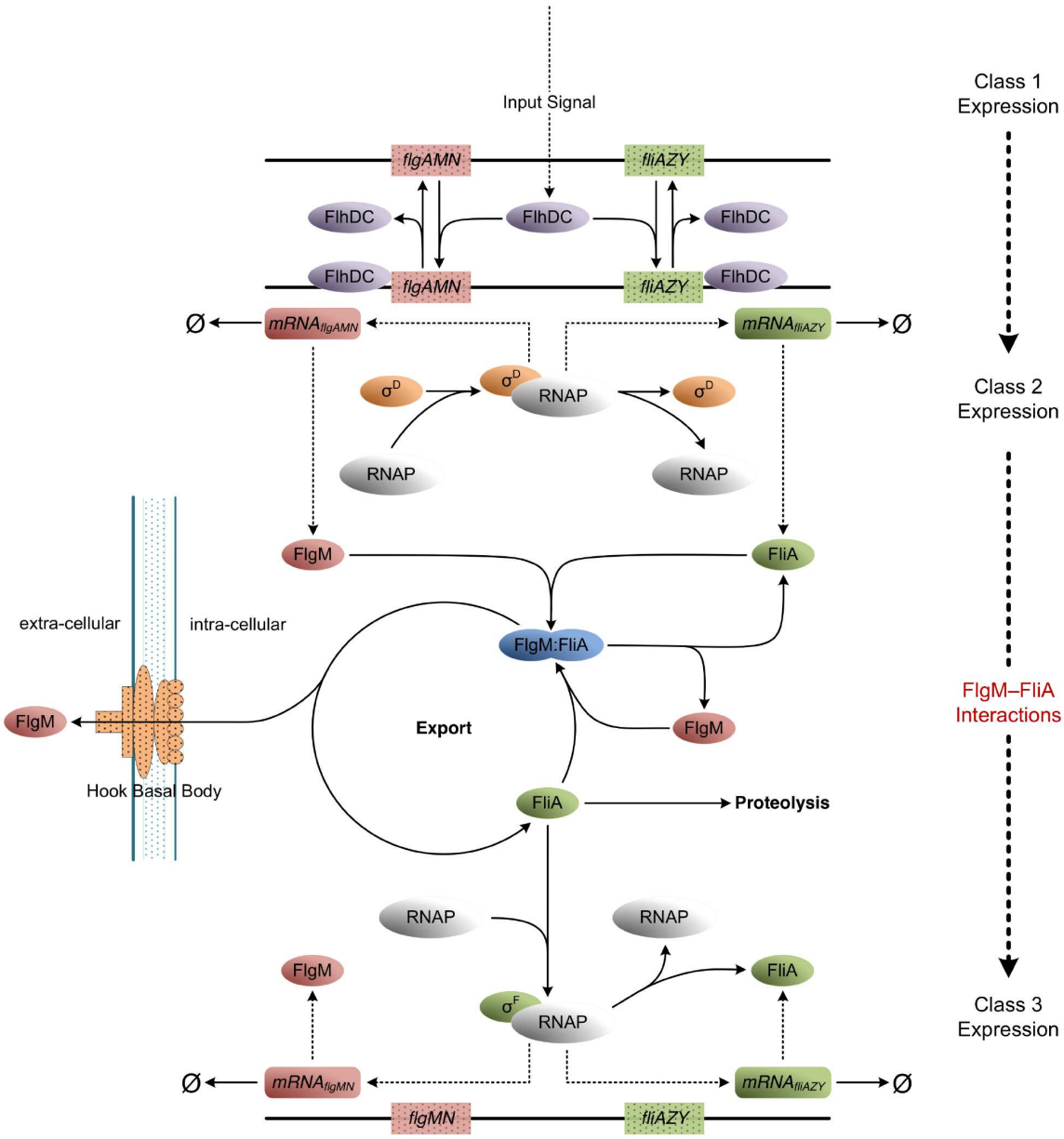

Figure 1. Model of the central flagellar checkpoint mechanism, including class 2 and class 3 gene expression. At the core are the direct interactions between FliA and FlgM, i.e., FlgM:FliA complex formation, FliA-mediated export of FlgM, FliA binding to RNAP and proteolysis of FliA. Important regulatory processes at the transcriptional and translational level are also included. Arrows do not indicate transcriptional direction on the chromosome.

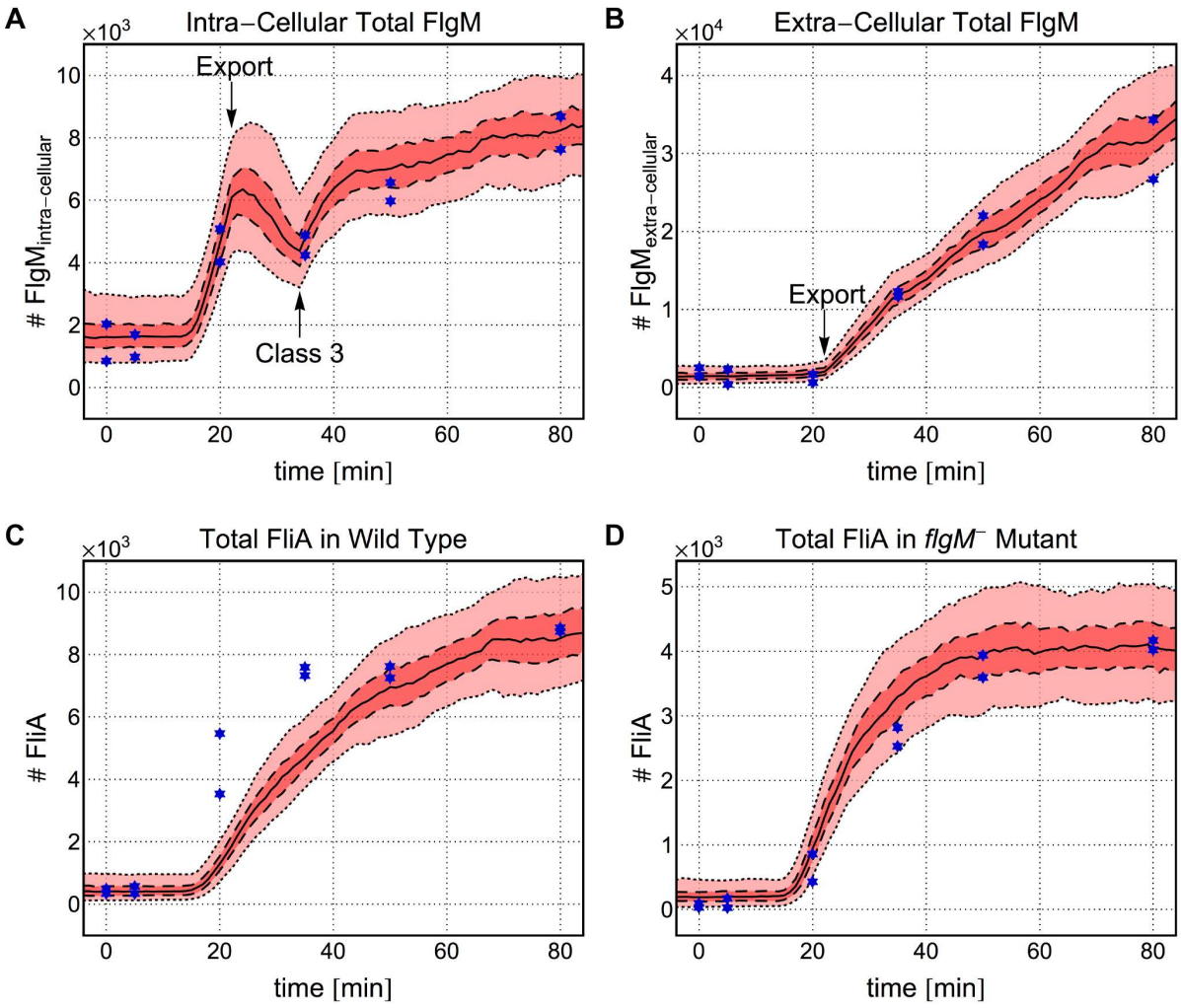

Figure 2. ***In silico*** **predictions based on the detailed stochastic model in comparison to** ***in vivo*** **measurements. Wild type**: (A) total intra-cellular numbers of FlgM molecules (free FlgM plus FlgM:FliA), (B) extra-cellular FlgM number of molecules, and (C) total number of FliA molecules (free FliA plus FlgM:FliA plus σ^{F}:RNAP) vs. time. ***flgM*** **mutant**: (D) total number of FliA molecules (free FliA plus σ^{F}:RNAP) vs. time. *In silico* data are depict by the model predictions of the median (solid lines), the area between the 40^{th} and 60^{th} percentile (dashed lines) and the area between the 1^{st} and 3^{rd} quartile ($25^{\mathrm{th}}/75^{\mathrm{th}}$ percentile, dotted lines). *In vivo* data are marked by '*', important events are marked: start of export (Export); and start of protein synthesis of class 3 gene products (Class 3).

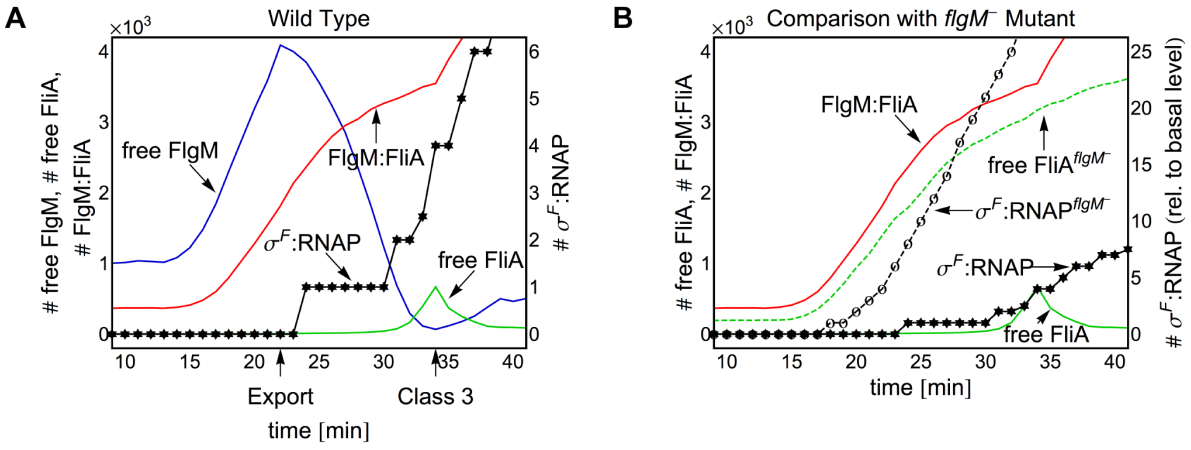

Figure 3. Analysis of the interaction between start of FlgM export and initiation of class 3 gene expression. Predictions based on the detailed stochastic model for free FlgM (—, blue), free FliA (—, green), FlgM:FliA complex (—, red) and σ^{F}:RNAP complex (-∗-, black). For the wild type (A), the most pronounced change in terms of numbers of molecules is the rapid decrease in free FlgM upon start of export, but not as one might expect in the level of FlgM:FliA complexes.

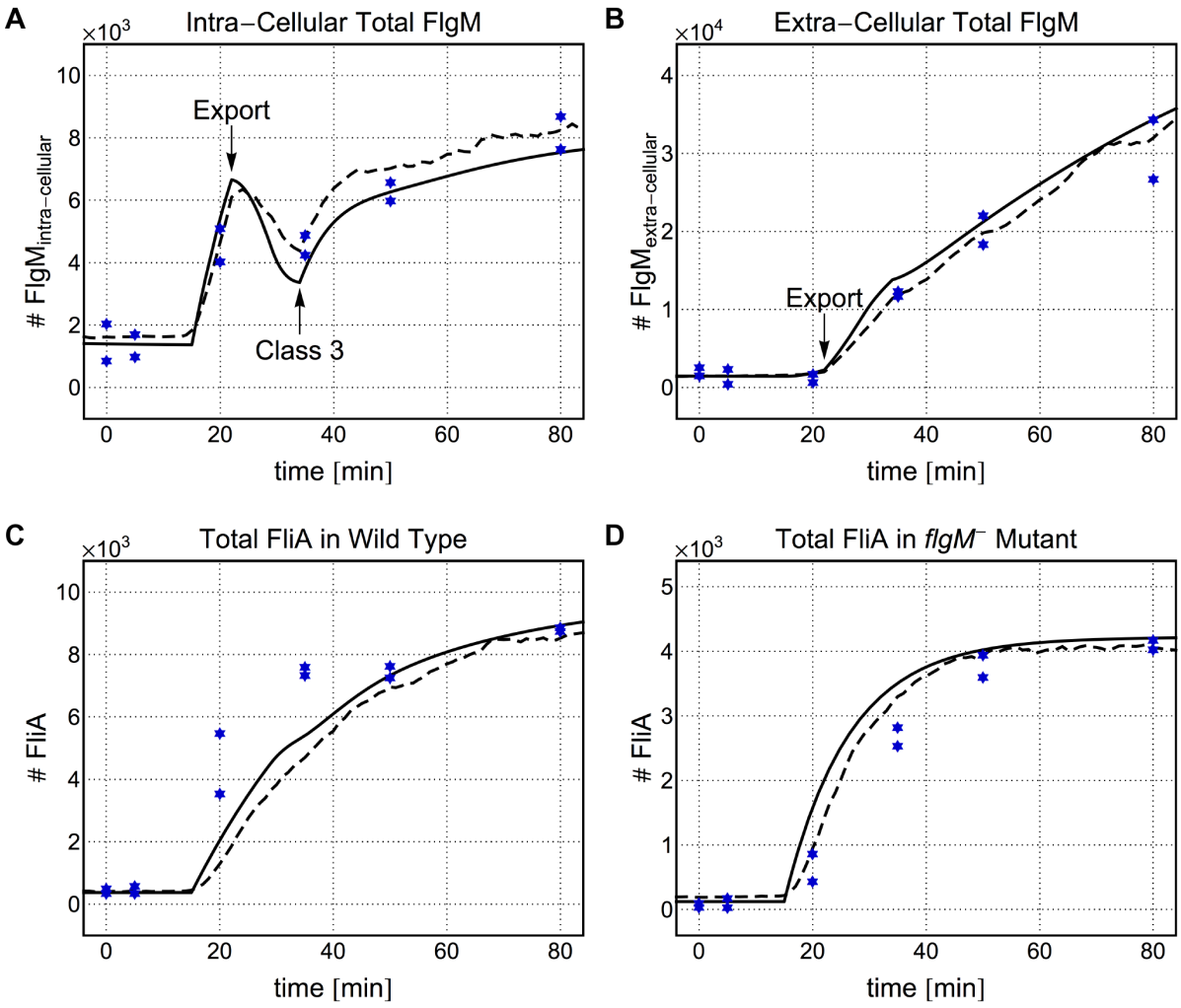

Figure 4. ***In silico*** **predictions based on the reduced deterministic model in comparison to** ***in vivo*** **measurements. Wild type**: (A) total intra-cellular FlgM (free FlgM plus FlgM:FliA), (B) extra-cellular FlgM, and (C) total FliA (free FliA plus FlgM:FliA plus σ^F:RNAP) vs. time. ***flgM*****⁻ mutant**: (D) total FliA (free FliA plus σ^F:RNAP) vs. time. The predictions of the reduced deterministic model (solid lines) are consistent with the mean levels (dashed lines) of the detailed stochastic model. Both basal and final levels as well as transient changes are in very good agreement. *In vivo* data are marked by '*', important events are marked: start of export (Export); and start of protein synthesis of class 3 gene products (Class 3).

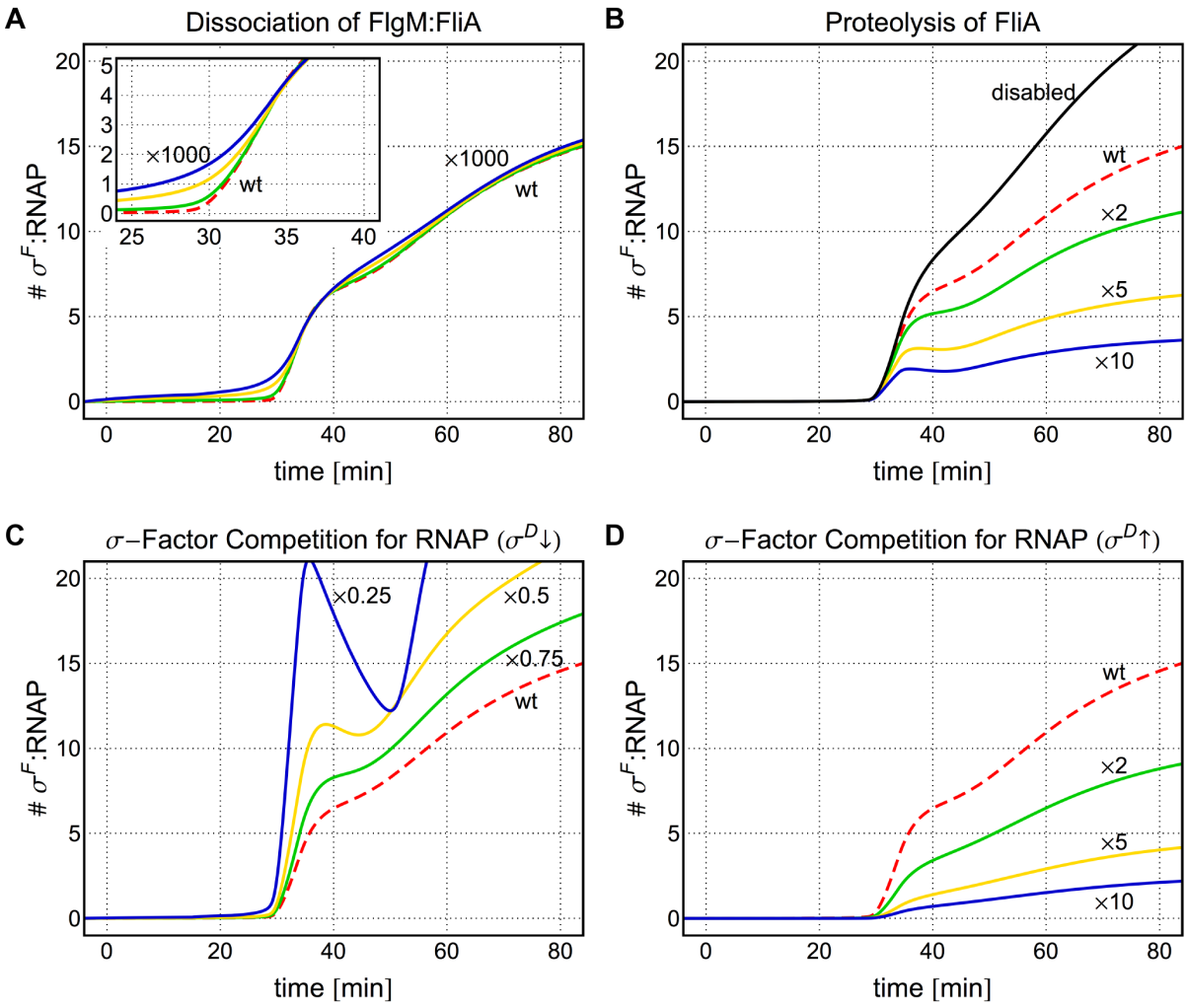

Figure 5. Predicted σ^{F}:RNAP levels for different *in silico* settings based on the reduced deterministic model. In each panel the σ^{F}:RNAP levels of the wild type (red, dashed line) is compared to levels of different *in silico* mutants (green, yellow and blue, solid lines) with 'perturbed' values in one parameter. (A) Dissociation constant k_{10} of the FlgM:FliA complex: 1-fold (red), 100-fold (green), 500-fold (yellow) and 1000-fold (blue) increase. (B) Rate constant k_4 of the FliA proteolysis: 1-fold (red), 2-fold (green), 5-fold (yellow) and 10-fold (blue) increase plus proteolysis disabled (black). (C) Total level of the sigma factor σ^{D}: 1-fold (red), 0.75-fold (green), 0.5-fold (yellow) and 0.25-fold (blue) decrease; and (D): 1-fold (red), 2-fold (green), 5-fold (yellow) and 10-fold (blue) increase.

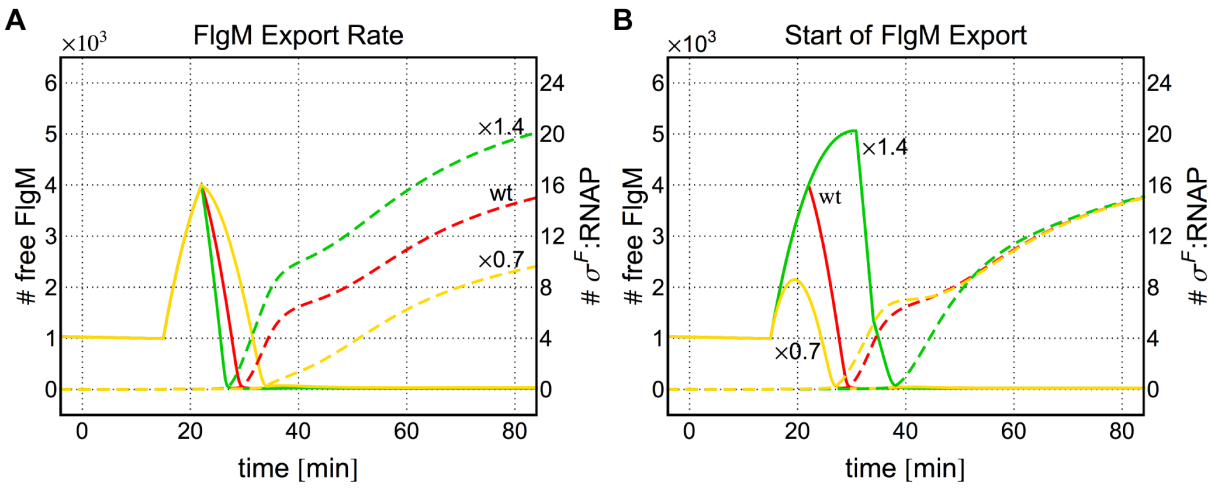

Figure 6. Predicted levels of free FlgM and σ^{F}:RNAP for different *in silico* settings of the FlgM export. (A) Effective FlgM export rate constant k_{11} and (B) starting time of FlgM export: 0.7-fold (yellow), 1-fold (red), and 1.4-fold (green). In each panel the free FlgM levels (solid lines) are related to the left scale, and the σ^{F}:RNAP levels (dashed lines) are related to the right scale.

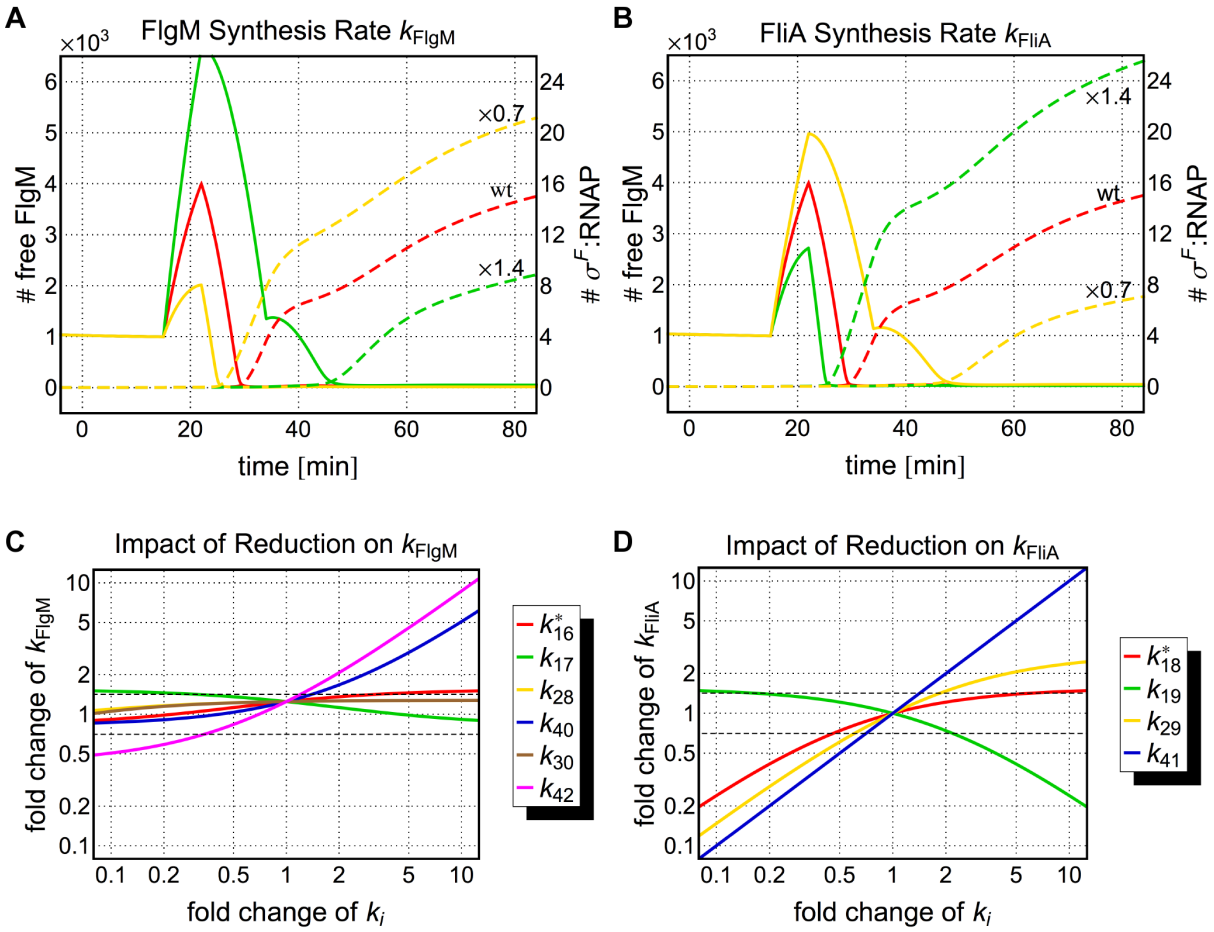

Figure 7. Sensitivity of the core regulatory mechanism to the effective synthesis rates of FlgM and FliA. Top: Predicted levels of free FlgM (solid lines, left scale) and σ^{F}:RNAP (dashed lines, right scale) for the wild type (red) and different *in silico* mutants (yellow and green). (A) FlgM synthesis rate constant k_{FlgM} and (B) the FliA synthesis rate constant k_{FliA}: 0.7-fold (yellow), 1-fold (red), and 1.4-fold (green). Bottom: Log-log plots of the effective production rates for FlgM (C) and FliA (D) in the reduced deterministic model with respect to changes in the subsumed rate constants of the detailed stochastic model. In (C) these are the average binding rate constant k^*_{16} and dissociation rate constant k_{17} of FlhDC to the class 2 promoter; the initiation rate constants of class 2 and class 3 transcription k_{28} and k_{30}, respectively; and the initiation rates of class 2 and class 3 translation k_{40} and k_{42}, respectively. In (D) these are the average binding rate constant k^*_{18} and dissociation rate constant k_{19} of FlhDC to the class 2 promoter; the initiation rate constant k_{29} of class 2 transcription; and the initiation rate constant k_{41} of class 2 translation. The dotted lines mark the variations of k_{FlgM} and k_{FliA} corresponding to the 0.7- and 1.4-fold change in the effective rate constants, shown in (A) and (B).

Table 1. Parameter values of the reduced deterministic model of the core regulatory mechanism

Rate Constant	Value	Unit
$k_{\mathrm{FlgM}}(t)$	$\begin{cases} 1.3 & \text{if } t \leq 15\,min \\ 17.4 + 6.3 \times 10^{-1} \cdot \sigma^{\mathrm{F}}\text{:RNAP} & \text{otherwise} \end{cases}$	$[\#molecules/s]$
$k_{\mathrm{FliA}}(t)$	$\begin{cases} 1.8 \times 10^{-1} & \text{if } t \leq 15\,min \\ 6.2 & \text{otherwise} \end{cases}$	$[\#molecules/s]$
k_4	1.0×10^{-3}	$\left[s^{-1}\right]$
k_9	7.4×10^{-4}	$\left[(\#molecules \cdot s)^{-1}\right]$
k_{10}	1.6×10^{-4}	$\left[s^{-1}\right]$
$k_{11}(t)$	$\begin{cases} 1.8 \times 10^{-3} & \text{if } t \leq 22\,min \\ 5.5 \times 10^{-3} & \text{if } 22\,min < t \leq 34\,min \\ 3.0 \times 10^{-3} & \text{otherwise} \end{cases}$	$\left[s^{-1}\right]$
k_{12}	2.1×10^{-4}	$\left[(\#molecules \cdot s)^{-1}\right]$
k_{13}	3.9×10^{-4}	$\left[s^{-1}\right]$
k_{14}	4.0×10^{-4}	$\left[(\#molecules \cdot s)^{-1}\right]$
k_{15}	3.9×10^{-4}	$\left[s^{-1}\right]$
k_{dil}	4.8×10^{-4}	$\left[s^{-1}\right]$

For derivation of $k_{\mathrm{FlgM}}(t)$, $k_{\mathrm{FliA}}(t)$ and k_{dil}, see Materials and Methods. All other rate constants and parameter values are identical to those listed for the detailed stochastic model, see Table S2 in the Supporting Information. Initial molecule numbers (based on stochastic simulations) for wild type: FlgM(0) = 712, FliA(0) = 1, FlgM:FliA(0) = 375, $\mathrm{FlgM}_{\mathrm{extern}}(0) = 1452$, $\sigma^{\mathrm{D}}(0) = 14900$, σ^{D}:RNAP(0) = 2100, all others zero; for *flgM*$^{-}$ mutant: FliA(0) = 121, σ^{F}:RNAP(0) = 1, $\sigma^{\mathrm{D}}(0) = 14902$, σ^{D}:RNAP(0) = 2099, all others zero.